Manipulation of Mg^{2+}- Ca^{2+} switch on the development of bone mimetic hydroxyapatite

*Nancy C. Andrés [a§], Noelia L. D´Elía [a§], Juan M. Ruso [b], Adrián E. Campelo[c], Virginia L. Massheimer[c], Paula V. Messina [a]**

(a) INQUISUR – CONICET, Department of Chemistry, Universidad Nacional del Sur, B8000CPB, Bahía Blanca, Argentina. (b) Soft Matter and Molecular Biophysics Group, Department of Applied Physics, University of Santiago de Compostela, Santiago de Compostela, 15782, Spain. (c) INBIOSUR - CONICET, DBByF, Universidad Nacional del Sur, B8000ICN, Bahía Blanca, Argentina

* Author to whom correspondence should be addressed. Tel: +54 291 4595159. Fax: +54 291 4595160. Electronic mail: pmessina@uns.edu.ar.

§ These authors contributed equally to this work, and should be considered as co-first authors.

In vitro hydrolytic and enzymatic degradation

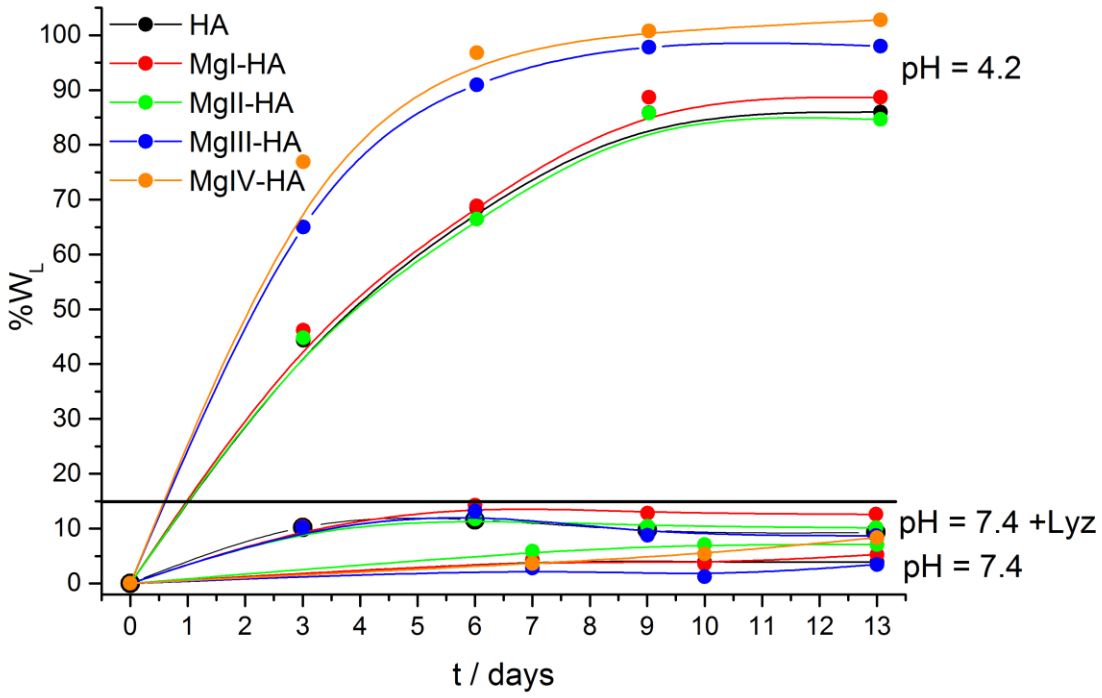

Figure S1. HA and Mg^{2+}- HA materials solubility under the action of different medias (physiological conditions at pH = 7.4; enzymatic degradation, pH=7.4 and Lysozyme; bone resorption conditions at pH 4.2.) at 37°C. After 10 days of treatment under physiological conditions (with or without the presence of Lysozyme) the materials reached the complete dissolution equilibria.

EDX-Microanalysis

MgI-HA

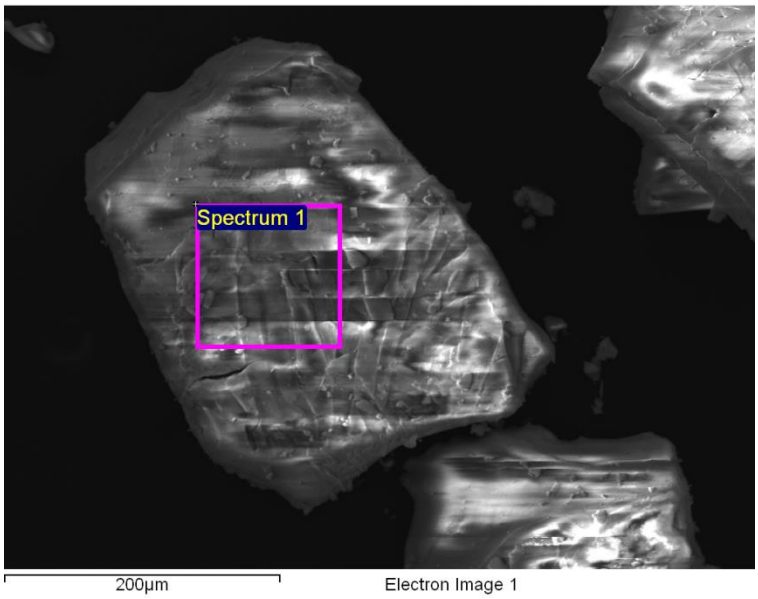

Spectrum processing :

Element	Weight%	Atomic%
C K	5.67	10.27
O K	42.98	58.42
Na K	1.05	1.00
Mg K	0.59	0.53
P K	17.68	12.41
Ca K	32.02	17.38
Totals	100.00	

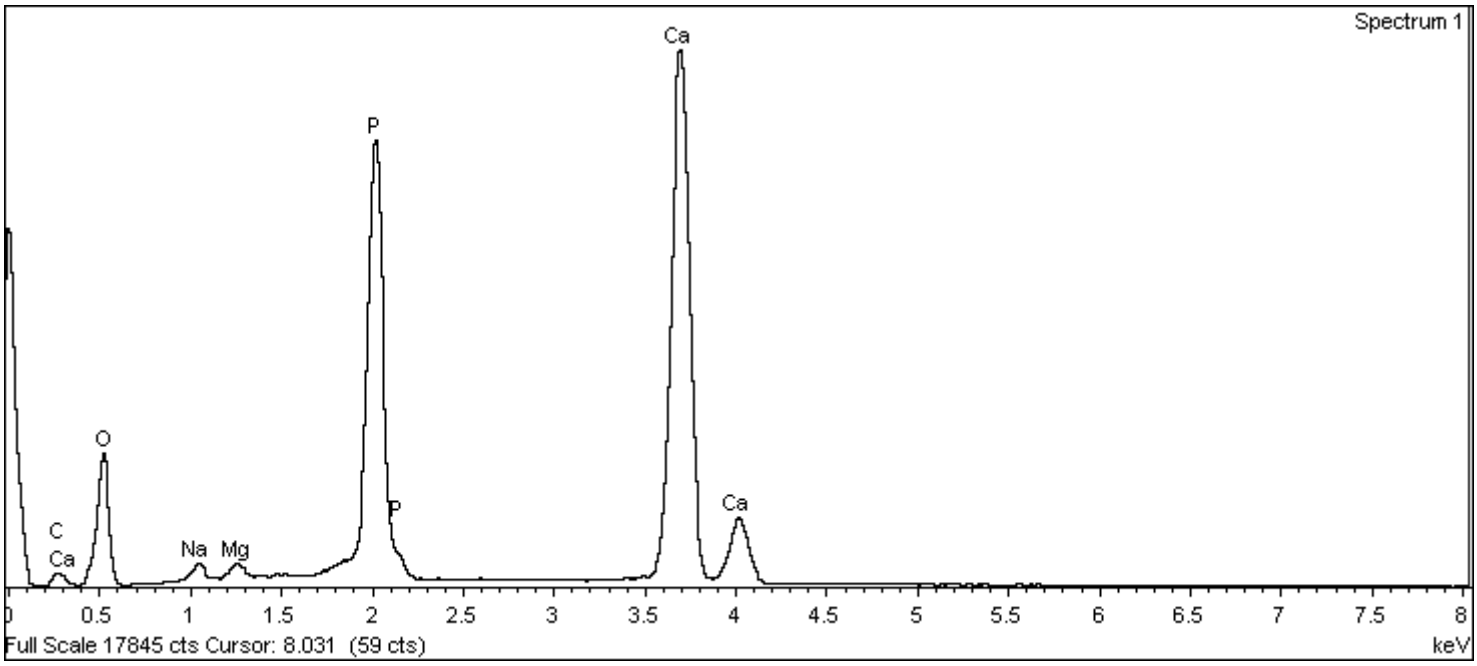

Figure S2. EDX-Microanalysis of MgI-HA material

MgII-HA

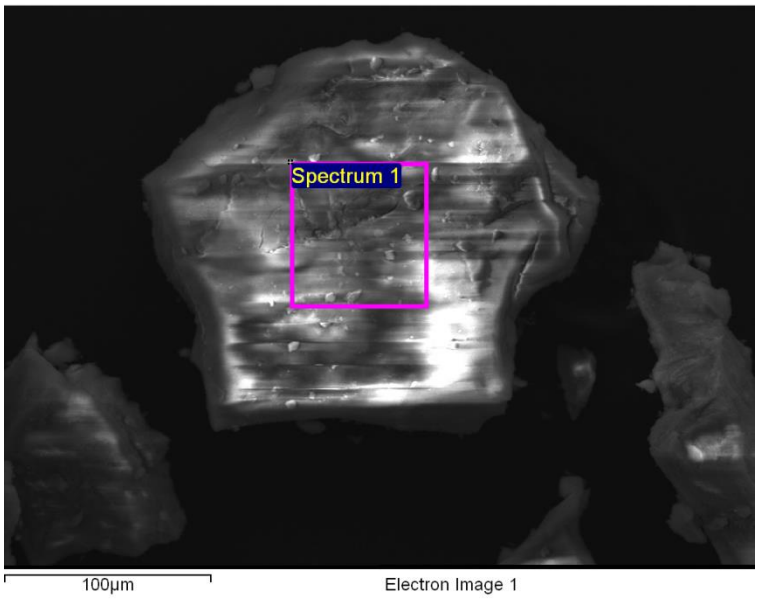

Spectrum processing :

Element	Weight%	Atomic%
C K	5.38	9.94
O K	40.37	56.00
Na K	1.52	1.47
Mg K	1.12	1.02
P K	18.35	13.15
Ca K	33.27	18.42
Totals	100.00	

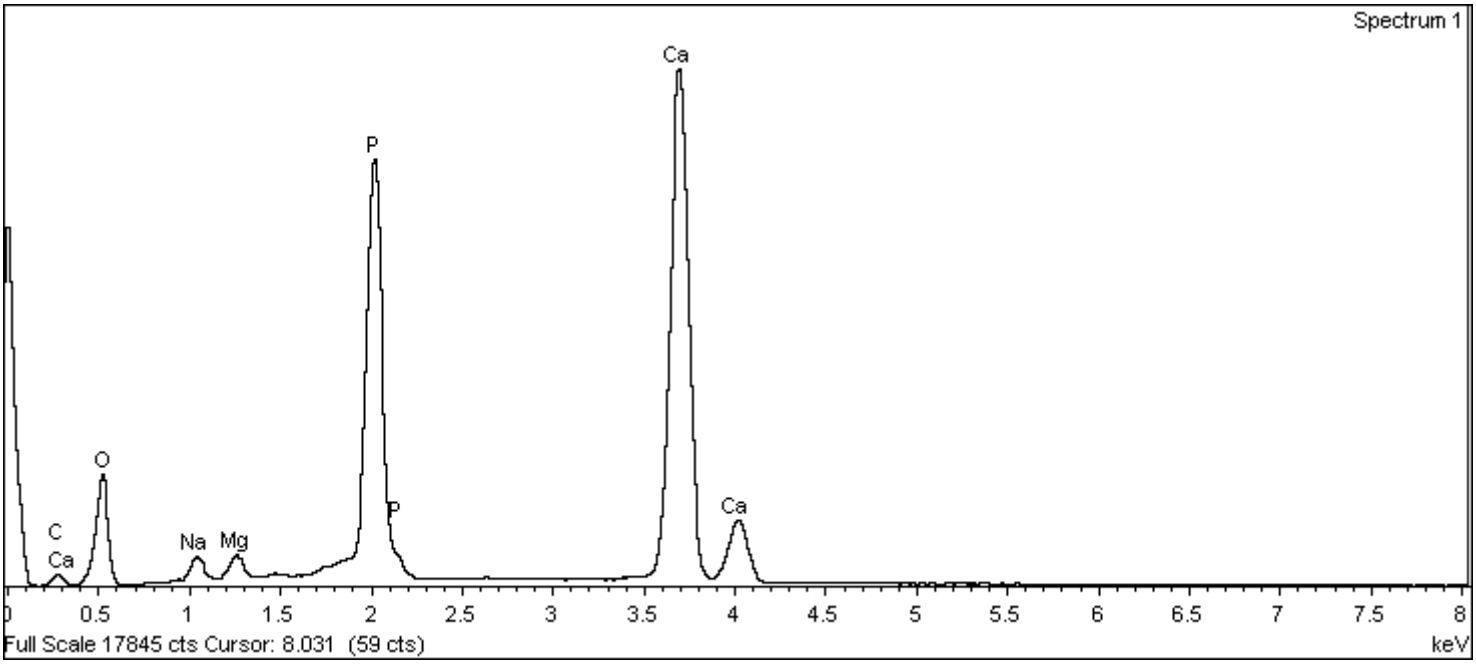

Figure S3. EDX-Microanalysis of MgII-HA material

MgIII-HA

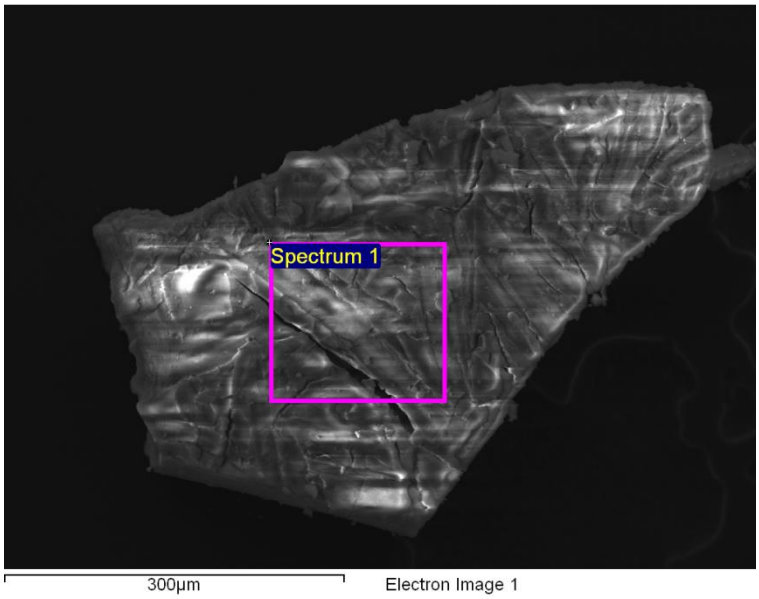

Spectrum processing :

Element	Weight%	Atomic%
C K	5.66	9.94
O K	46.21	60.89
Na K	1.26	1.16
Mg K	2.12	1.83
P K	17.07	11.62
Ca K	27.68	14.56
Totals	100.00	

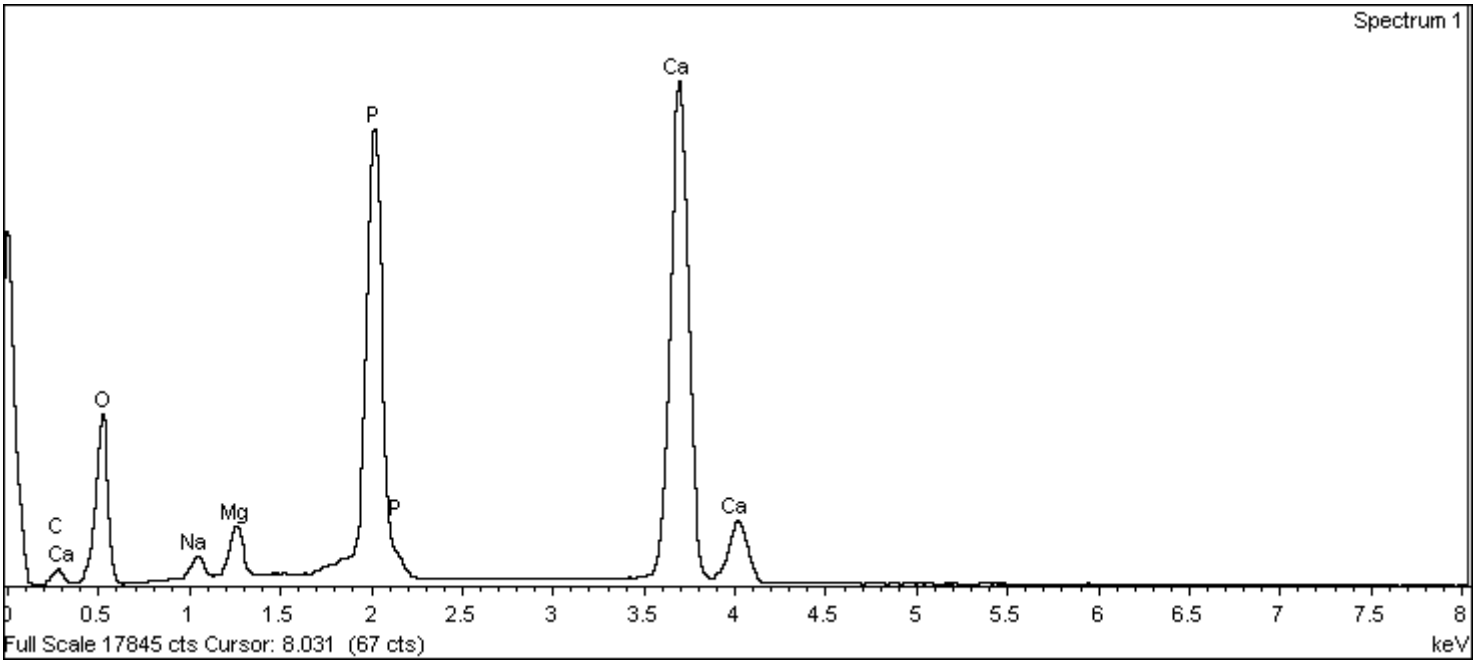

Figure S4. EDX-Microanalysis of MgIII-HA material

MgIV-HA

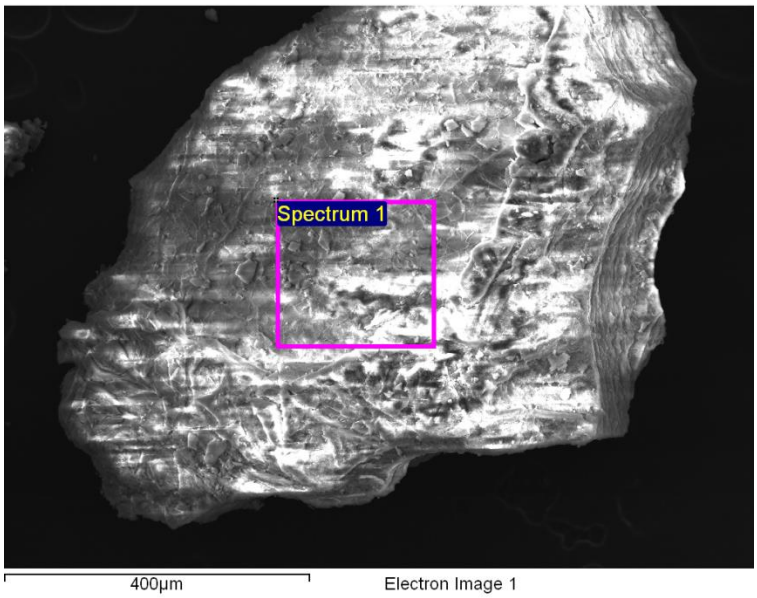

Spectrum processing :

Element	Weight%	Atomic%
C K	5.45	9.31
O K	46.92	60.22
Na K	0.76	0.68
Mg K	6.13	5.18
Al K	0.31	0.24
P K	12.06	7.99
Ca K	19.94	10.22
Totals	100.00	

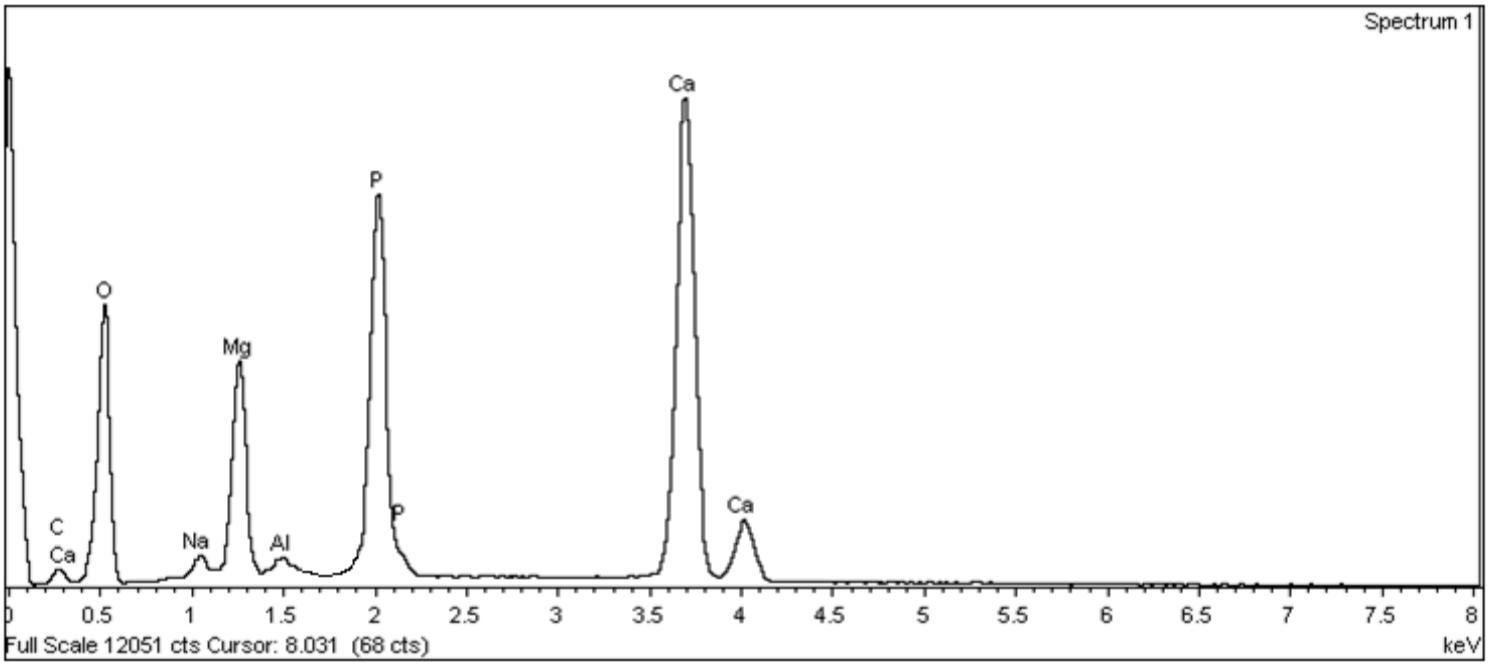

Figure S5. EDX-Microanalysis of MgIV-HA material

Molecular modeling

Atomic coordinates and isotropic displacement parameters (in $Å^2$):

Table S1. Stoichiometric HA crystallographic unit cell

Atom	Ox.	Wyck.	x	y	z	B
Ca1	+2	4f	2/3	1/3	0.01030	1.3000
Ca2	+2	6h	0.24627	0.23737	1/4	1.3000
P1	+3	6h	0.02886	0.40568	1/4	1.3000
O1	-2	12i	0.07903	0.34479	0.05933	1.3000
O2	-2	6h	0.49079	0.15330	1/4	1.3000
O3	-2	6h	0.12872	0.59834	1/4	1.3000
O4	-2	2a	0	0	1/4	1.3000

Table S2. Mg^{2+}- HA Ca6Mg4P6O26 crystallographic unit cell

Atom	Ox.	Wyck.	x	y	z	B
P1	+3	6h	0.02259	0.41895	1/4	1.3000
O1	-2	12i	0.05612	0.34161	0.05933	1.3000
O2	-2	6h	0.52711	0.16053	1/4	1.3000
O3	-2	6h	0.14006	0.60830	1/4	1.3000
O4	-2	2b	0	0	0	1.3000
Mg1	+2	4f	2/3	1/3	0.02689	1.3000
Ca1	+2	6h	0.22532	0.22238	1/4	1.3000

Table S3. Defective Mg^{2+}- HA Ca6 Mg4 P6 O26 crystallographic unit cell

Atom	Ox.	Wyck.	x	y	z	B
Ca1	+2	6h	0.03163	0.23436	1/4	
Mg1	+2	4f	1/3	2/3	0.00272	
P1	+3	6h	0.63046	0.00175	1/4	
O1	-2	12i	0.25171	0.36022	0.09128	
O2	-2	6h	0.47054	0.01782	1/4	
O3	-2	6h	0.44175	0.21980	1/4	
O4	-2	2b	0	0	0	

Rietveld refinement

MgI-HA

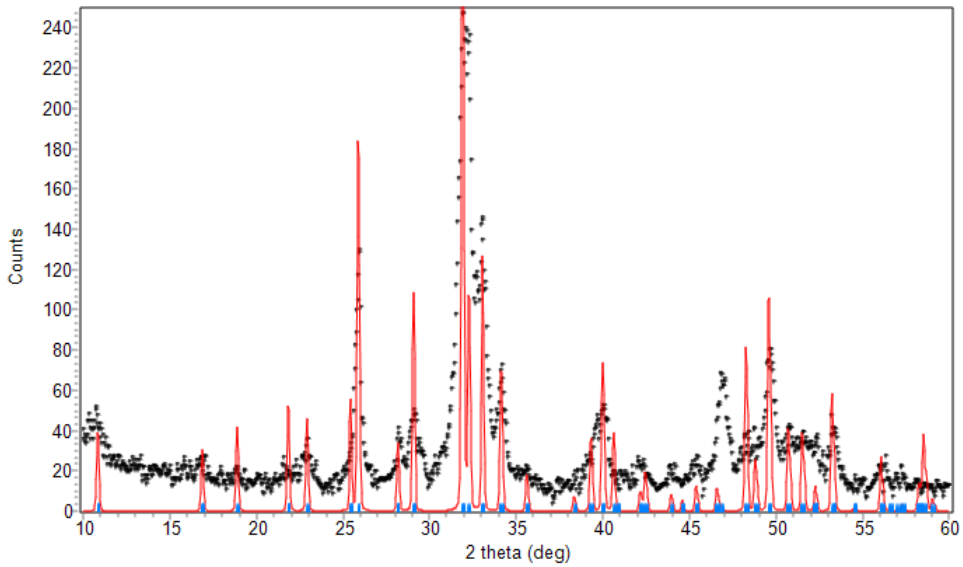

Figure S6. X-ray diffraction pattern of MgI-HA, black dots: experimental data; red line: theoretical data computed with Rietica v4.2 software package.

MgII-HA

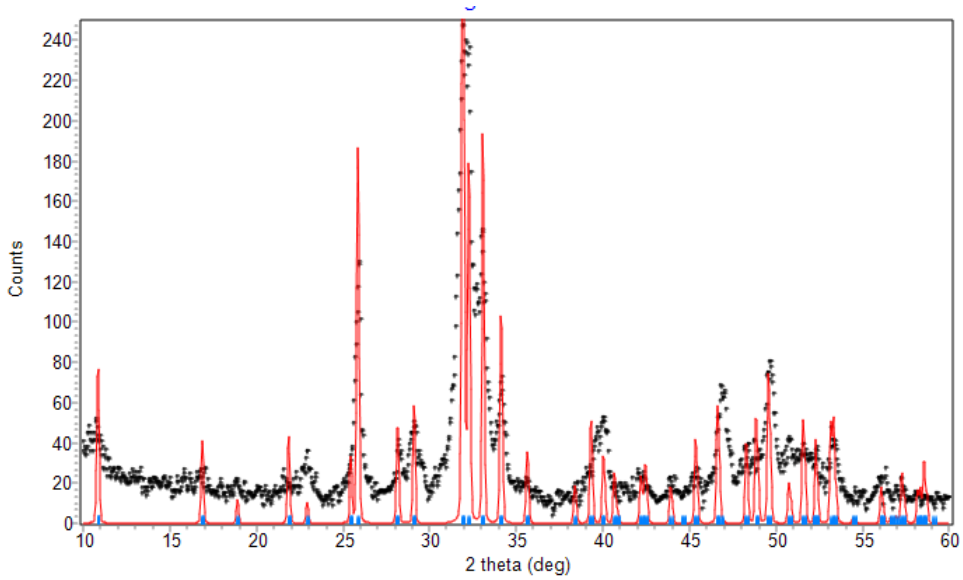

Figure S7. X-ray diffraction pattern of MgII-HA, black dots: experimental data; red line: theoretical data computed with Rietica v4.2 software package.

MgIII-HA

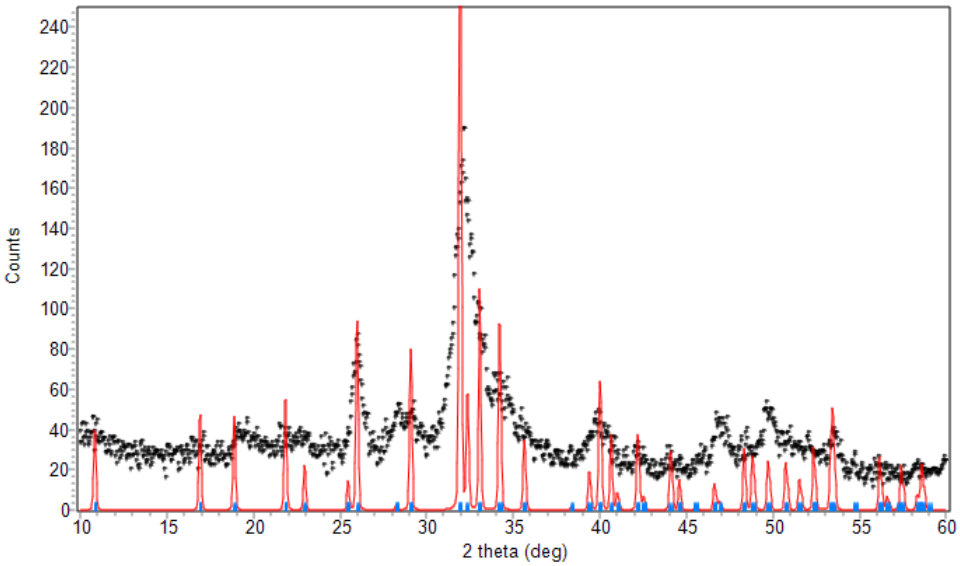

Figure S8. X-ray diffraction pattern of MgIII-HA, black dots: experimental data; red line: theoretical data computed with Rietica v4.2 software package.

MgIV-HA

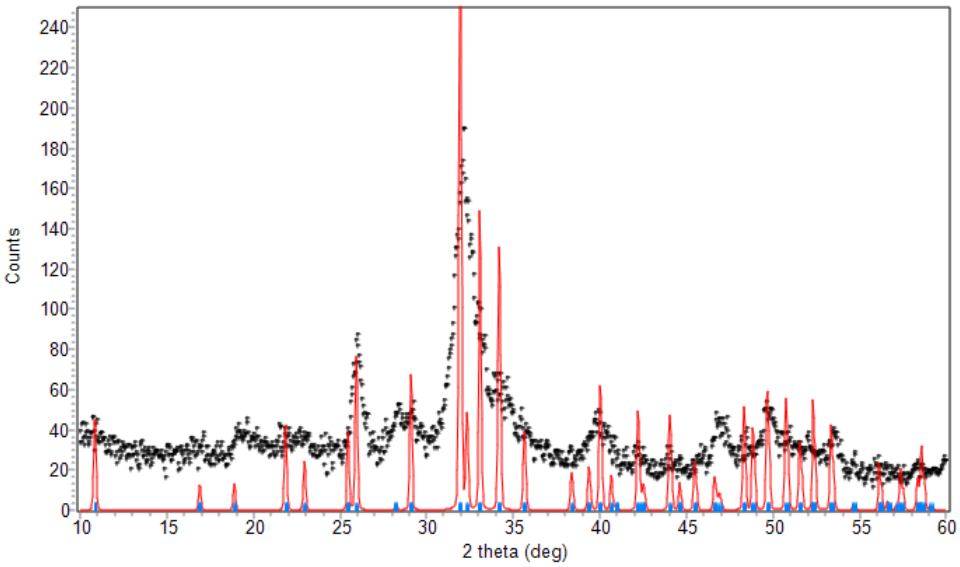

Figure S9. X-ray diffraction pattern of MgIV-HA, black dots: experimental data; red line: theoretical data computed with Rietica v4.2 software package.

Size distribution histograms

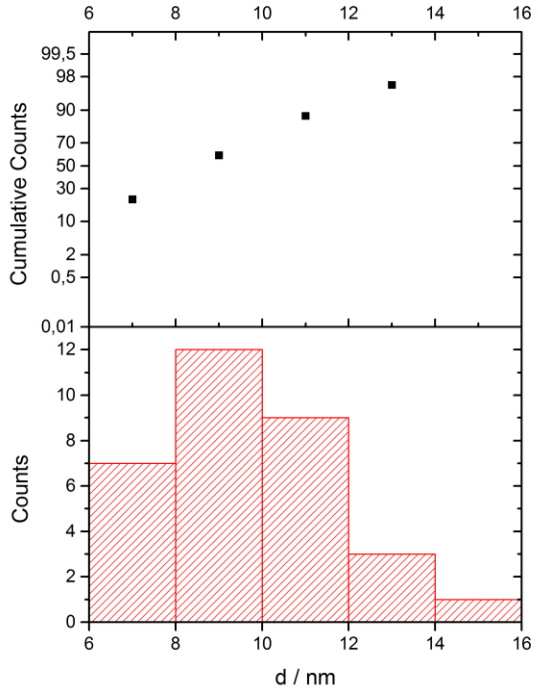

Figure S10. Diameter (*d*) distribution histogram of MgI-HA material

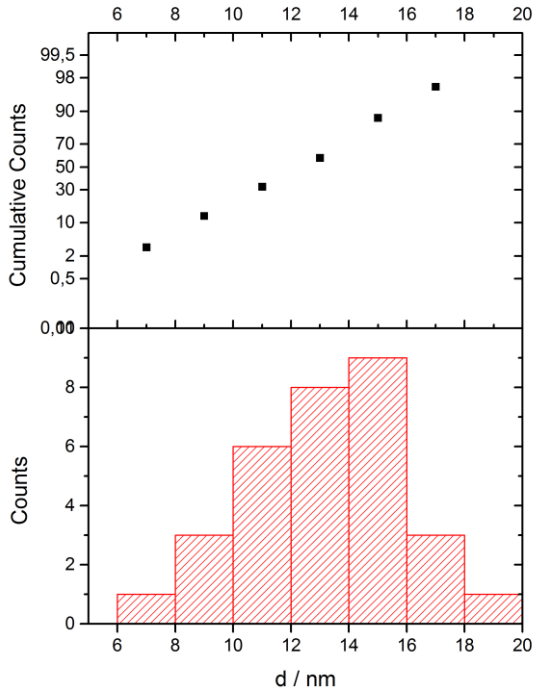

Figure S11. Diameter (*d*) distribution histogram of MgII-HA material

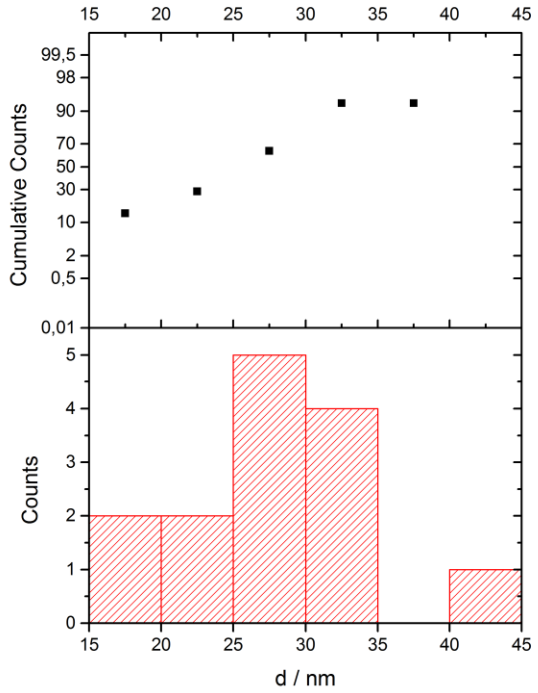

Figure S12. Diameter (*d*) distribution histogram of MgIII-HA material

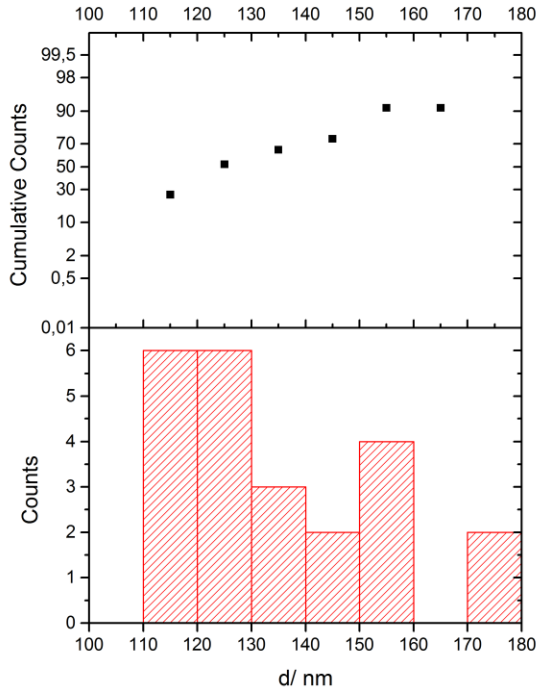

Figure S13. Diameter (*d*) distribution histogram of MgIV-HA material

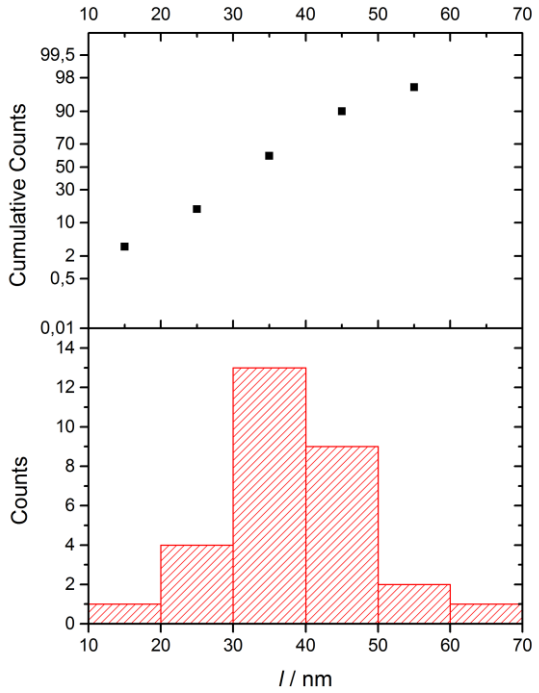

Figure S14. Length (*l*) distribution histogram of MgI-HA material

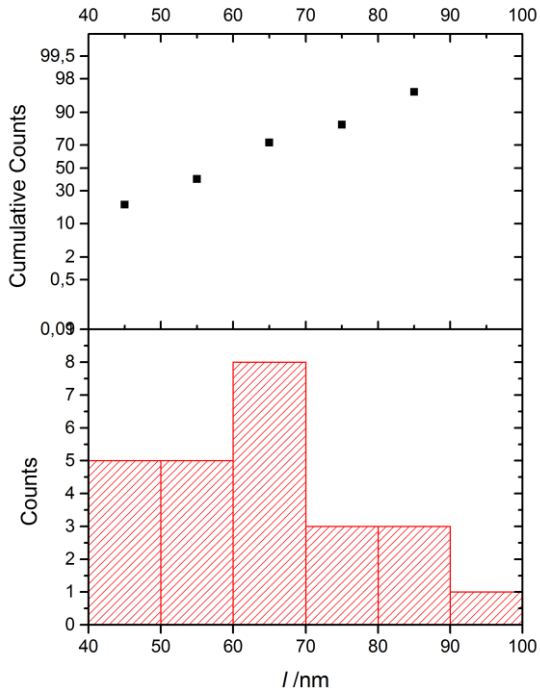

Figure S15. Length (*l*) distribution histogram of MgII-HA material

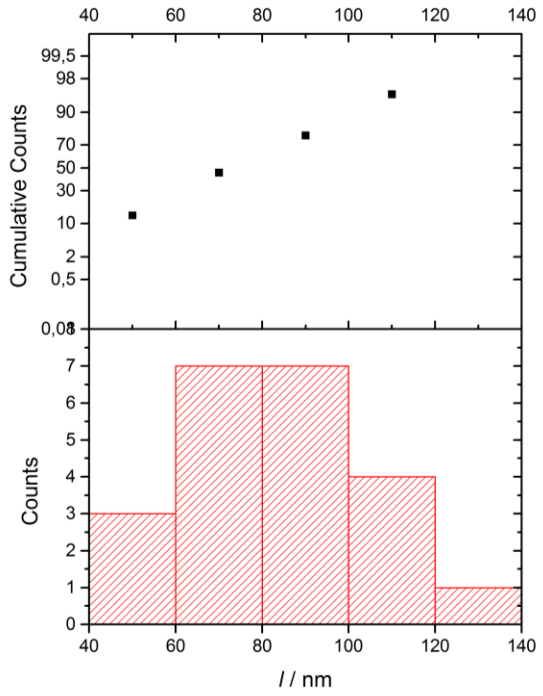

Figure S16. Length (*l*) distribution histogram of MgIII-HA material

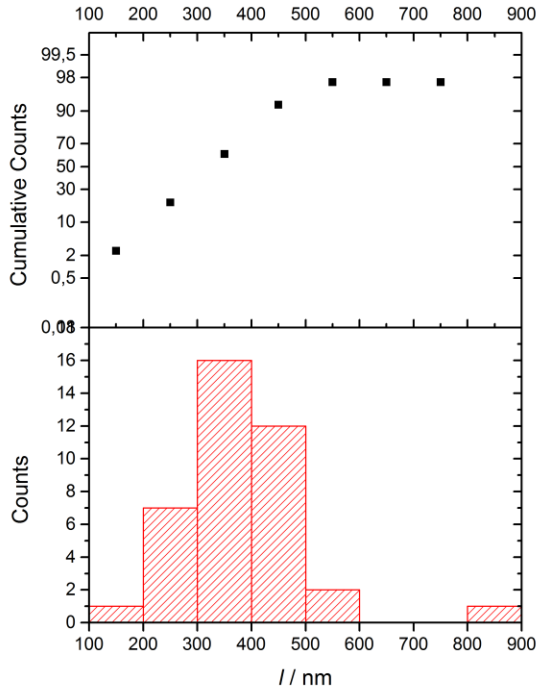

Figure S17. Length (*l*) distribution histogram of MgIV-HA material

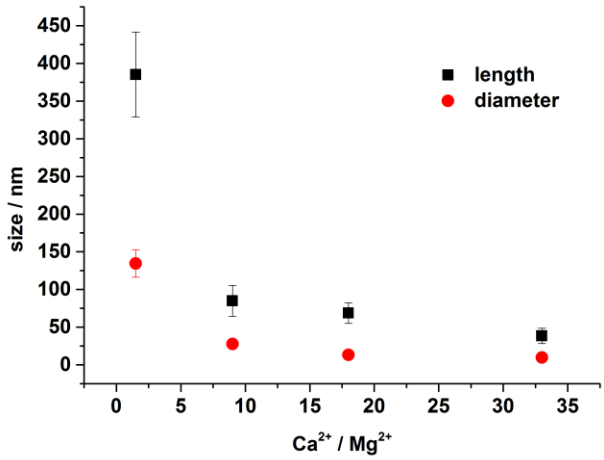

Figure S18. Summary of Mg^{2+}- HA nanoparticles' size dimensions as a function of Ca/Mg ratio.

Degradation under physiological and bone resorption conditions

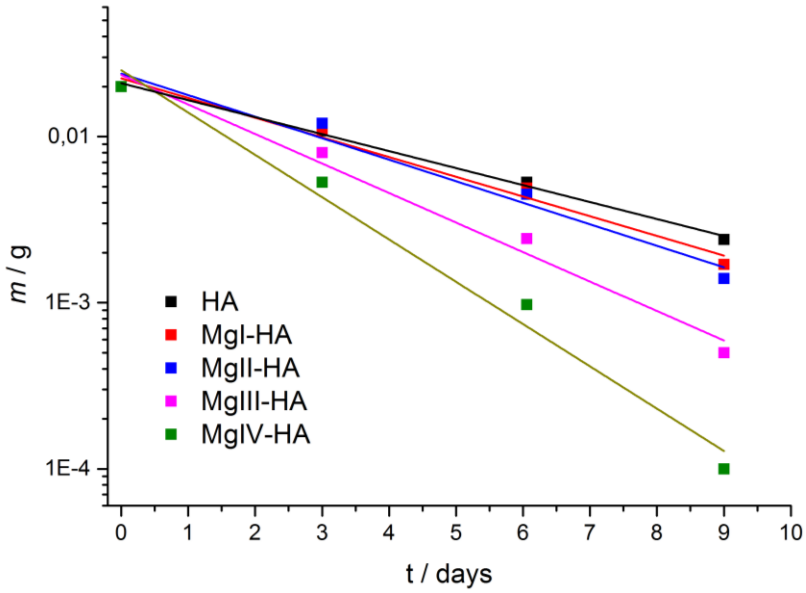

Figure S19. $log\left(\frac{m(t)}{m(0)}\right)$ *vs.* time plot

Cellular - material interactions

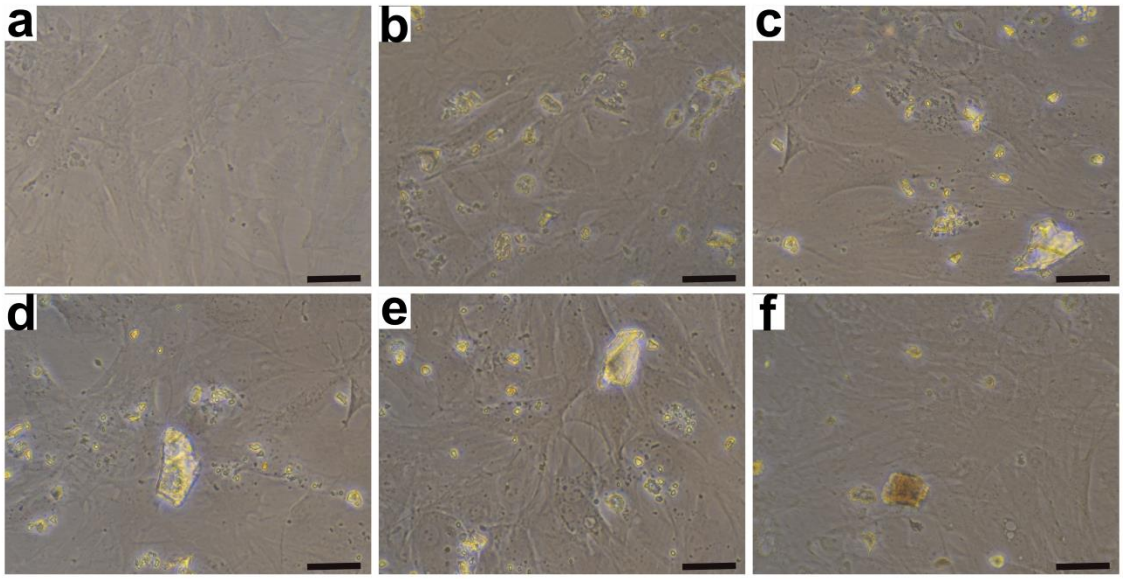

Figure S20. Phase contrast microphotographs of rOBs cultured in the presence of different Mg^{2+}- HA powders: (a) control; (b) HA; (c) MgI-HA; (d) MgII-HA; (e) MgIII-HA and (f) MgIV-HA. Scale bar: 100 μm. Bright spots: Mg^{2+}- HA powder.

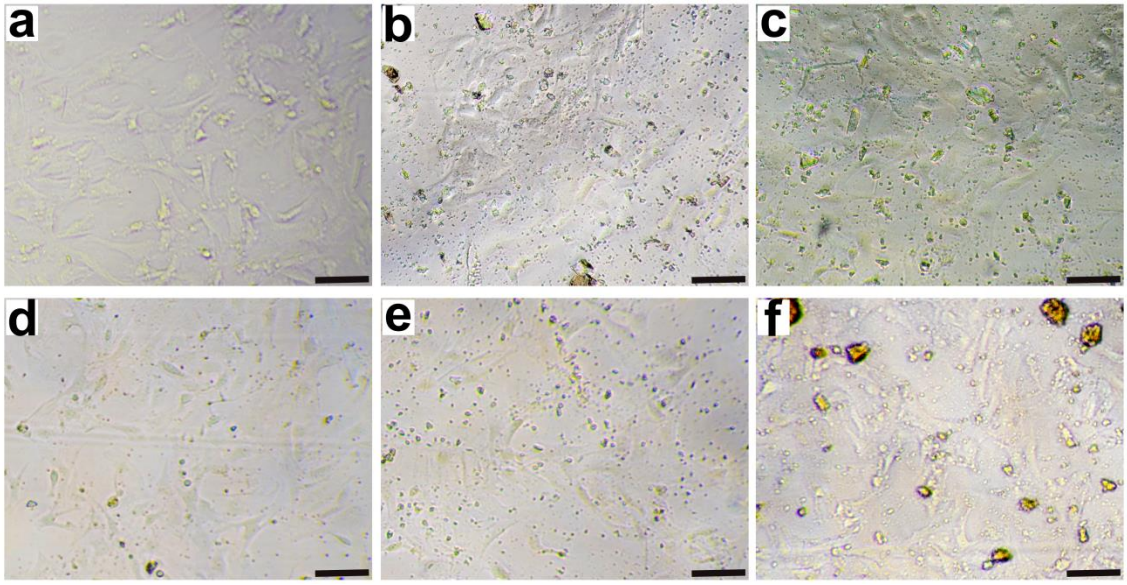

Figure S21. Phase contrast microphotographs of rECs cultured in the presence of different Mg^{2+}- HA powders: (a) control; (b) HA; (c) MgI-HA; (d) MgII-HA; (e) MgIII-HA and (f) MgIV-HA. Scale bar: 100 μm

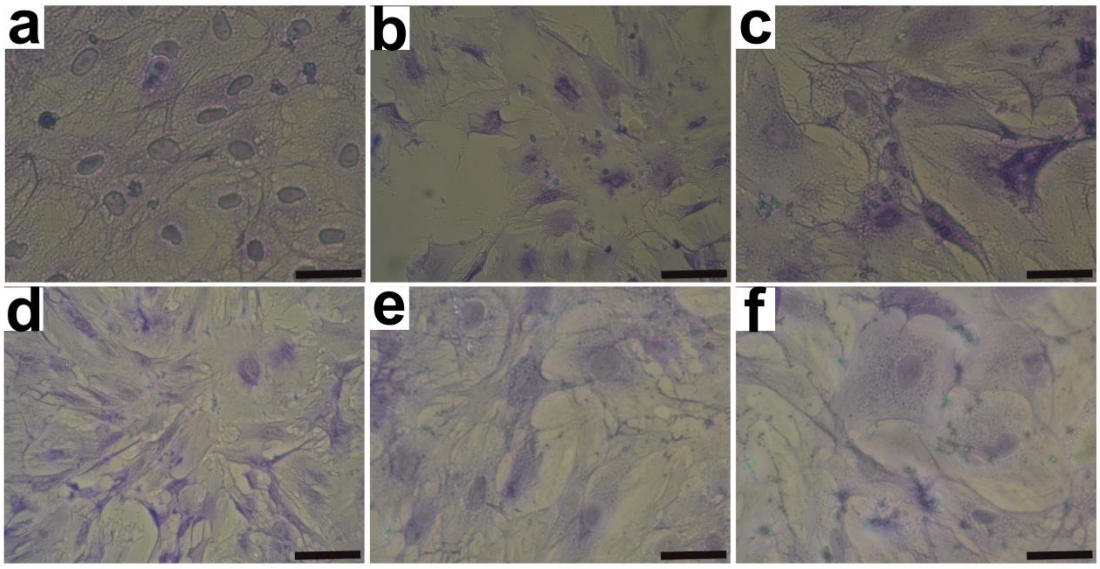

Figure S22. Crystal Violet staining (CVS) of rOBs cultured in the presence of different Mg^{2+}- HA powders: (a) control; (b) HA; (c) MgI-HA; (d) MgII-HA; (e) MgIII-HA and (f) MgIV-HA. Scale bar: 100 μm

Cellular morphology quantification

Cytomorphometric analysis was done using free ImageJ software accordingly to Foldberg et al. methodology.[1] For each cell, the area and length of the major and minor axis of an object equivalent ellipse were obtained. Then, the aspect ratio of each cell was calculated by dividing the major axis of the ellipse by the minor. **Figures S23-26** show examples of the calculations performed.

Figure S23. High contrast CVS microphotographs of rOBs cultured in the presence of MgIII-HA sample. Scale bar: 100 μm

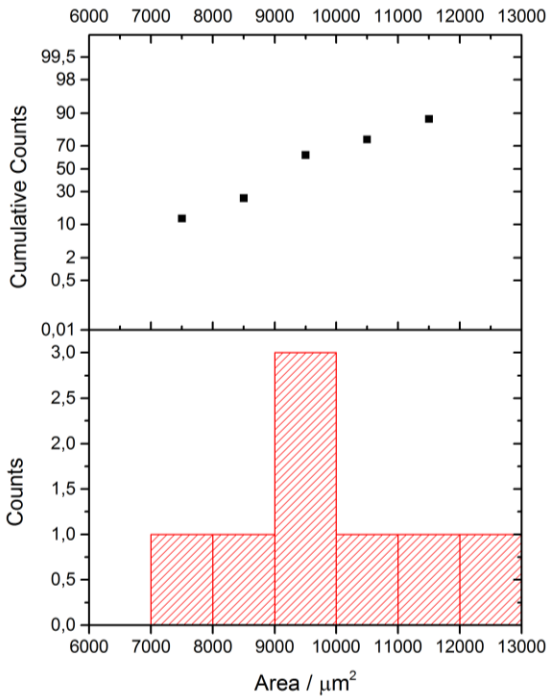

Figure S24. Histogram distribution of rOBs areas measured with ImageJ from figure S23.

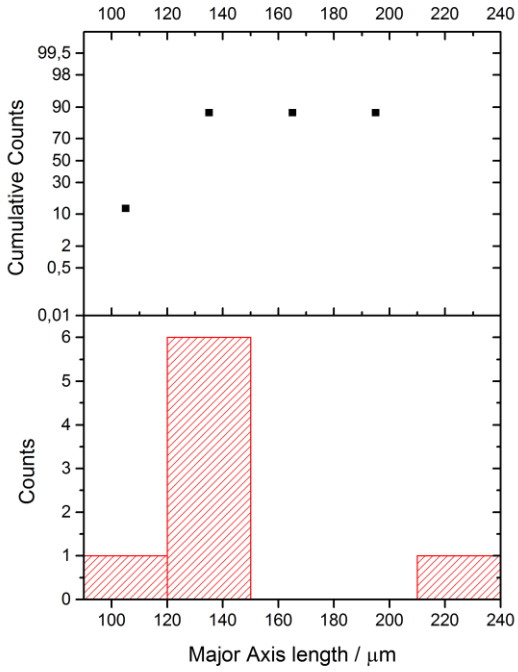

Figure S25. Histogram distribution of rOBs' major axis length measured with ImageJ from figure S23.

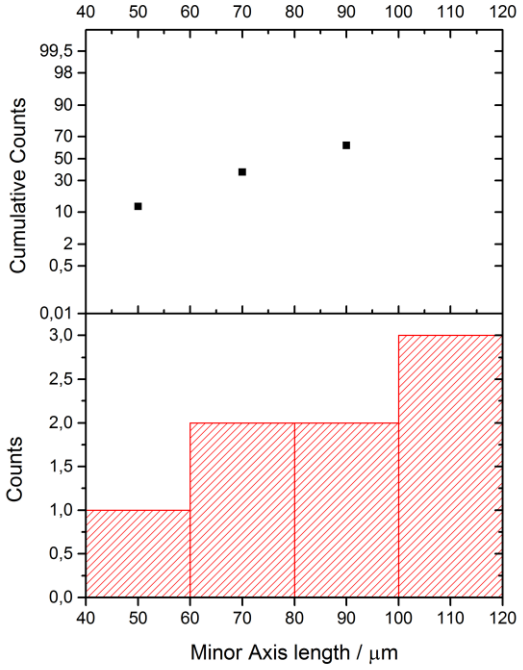

Figure S26. Histogram distribution of rOBs' minor axis length measured with ImageJ from figure S23.

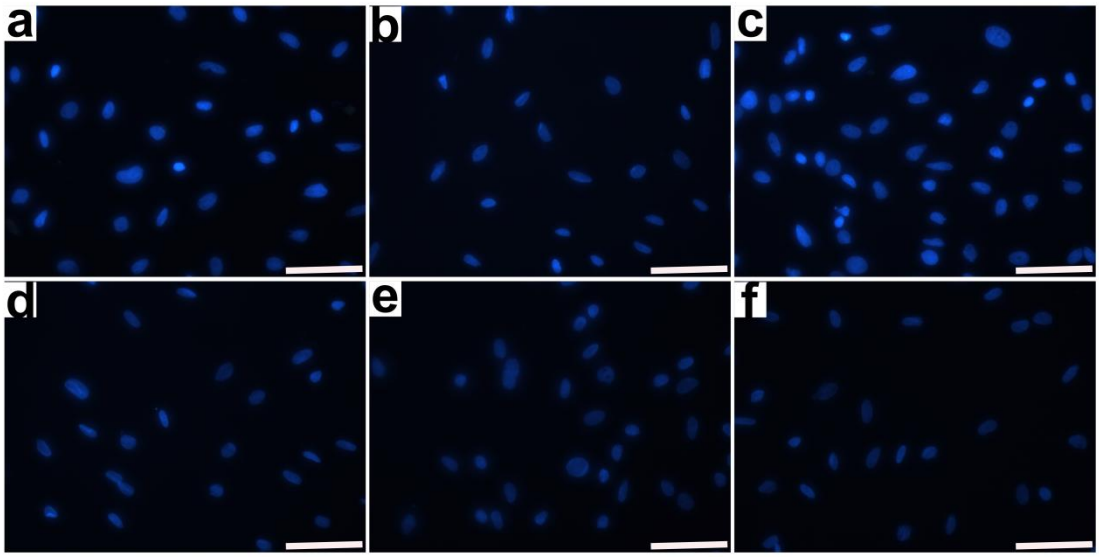

Figure S27. DAPI staining of rOBs nuclear DNA. Cells were cultured in the presence of different Mg^{2+}- HA powders: (a) control; (b) HA; (c) MgI-HA; (d) MgII-HA; (e) MgIII-HA and (f) MgIV-HA. Scale bar: 100 μm

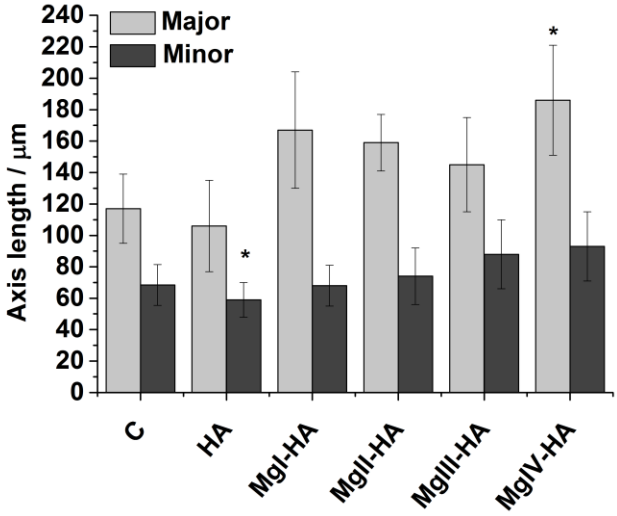

Figure S28. The charts show the length of the major and minor axis of rOBs cultured in the presence of Mg^{2+}- HA samples. Asterisks denote statistically significant differences (*$p < 0.05$).

References

(1) Foldberg, S.; Petersen, M.; Fojan, P.; Gurevich, L.; Fink, T.; Pennisi, C. P.; Zachar, V. Patterned poly(lactic acid) Films Support Growth and Spontaneous Multilineage Gene Expression of Adipose-derived Stem Cells. *Colloids Surf., B* **2012,** *93*, 92-99.